2015

# Signature predictions of surface targets undergoing turning maneuvers in spotlight synthetic aperture radar imagery

Garren, David A.

Garren, David A. "Signature predictions of surface targets undergoing turning maneuvers in spotlight synthetic aperture radar imagery." In Algorithms for Synthetic Aperture Radar Imagery XXII, vol. 9475, p. 94750A. International Society for Optics and Photonics, 2015.

https://hdl.handle.net/10945/59006

# Signature predictions of surface targets undergoing turning maneuvers in spotlight synthetic aperture radar imagery

David A. Garren

David A. Garren, "Signature predictions of surface targets undergoing turning maneuvers in spotlight synthetic aperture radar imagery," Proc. SPIE 9475, Algorithms for Synthetic Aperture Radar Imagery XXII, 94750A (13 May 2015); doi: 10.1117/12.2177372

SPIE.

Event: SPIE Defense + Security, 2015, Baltimore, Maryland, United States

# Signature Predictions of Surface Targets Undergoing Turning Maneuvers in Spotlight Synthetic Aperture Radar Imagery

David A. Garren

Department of Electrical and Computer Engineering
Naval Postgraduate School, Monterey, CA 93943, USA

## ABSTRACT

This paper investigates methodologies for predicting the smear signatures in broadside spotlight synthetic aperture radar imagery collections due to surface targets that are undergoing turning maneuvers. This analysis examines the case of broadside geometry wherein the radar moves with constant speed and heading on a level flight path. This investigation concentrates moving target smear issues that yield some defocus in the range direction, although much smaller in magnitude than the motion induced smearing in the radar cross-range direction. This paper focuses on the case of a target that executes a turning maneuver during the SAR collection interval. The SAR simulations are shown to give excellent agreement between the moving target signatures and the predicted shapes of the central contours.

**Keywords:** Synthetic aperture radar, Low probability of intercept, Radar imaging, Radar theory

## 1. INTRODUCTION

This paper investigates methodologies for predicting the smear signatures in broadside spotlight synthetic aperture radar (SAR) imagery collections due to surface targets that are undergoing turning maneuvers. Analytic computation of a power series expansion of the subaperture phase function[1] is used to compute a generic expression for the down-range and cross-range components of the predicted mover signature.

Studies of moving target signatures in SAR have revealed that the primary component of the smearing lies in the radar cross-range direction. However, there is also a slight component in the radar down-range direction, yielding moving target signatures that frequently have a curved or bowed shape. In fact, the details of the target motion and the radar collection contribute to the resulting location, extent, and shape of the resulting smear. One of the elements of the smear shape is whether the signature is curved upwards like a bowl towards near range or curved downwards like a hill towards far range.

The analytic expressions for the signature contours of turning targets are considered for typical SAR collections. The turning motion of a surface target introduces additional terms into the signature equations that can induce significant effects upon the resulting smear. In fact, these effects can reverse the concavity of a curved smear relative to a target that is moving with constant speed and heading. Examples are presented to demonstrate that these signature prediction equations yield excellent agreement with simulated SAR smears. Therefore, these general signature prediction equations can provide an effective tool in predicting the shape, extent, and location of signature smears due to turning surface targets.

The smearing of moving target signatures smeared signatures has been investigated by numerous researchers. For example, Perry et al.[2] generates refocused target signatures by using the smeared signatures of moving targets. These techniques assume that the smearing lies entirely in the radar cross-range direction, which is an assumption that has been made with many other studies. In addition, the general properties of moving target signatures within SAR imagery has been analyzed.[3]

For narrow-band SAR, the signature lies almost primarily in the radar cross-range direction. However, if the radar bandwidth is a significant fraction of the center frequency, then the mover signature can exhibit smearing effects in the radar down-range direction as well. Jao[4] has shown that moving target signatures can exhibit

Further author information: (Send correspondence to David A. Garren)
David A. Garren: E-mail: dagarren@nps.edu

Algorithms for Synthetic Aperture Radar Imagery XXII, edited by Edmund Zelnio, Frederick D. Garber, Proc. of SPIE Vol. 9475, 94750A · © 2015 SPIE
CCC code: 0277-786X/15/$18 · doi: 10.1117/12.2177372

a basic curved bowing shape, while being consistent with the result that the smearing still lies in the radar cross-range direction. The signature bowing can be either concave up or concave down, depending upon the particular details of the target heading and the platform motion. These "target migration" effects are of interest in understanding the motion of surface targets based upon their signatures within SAR imagery.

Stolt[5] has developed methods for compensating the effects of range migration via special interpolation techniques. This methodology can be applied in the focusing of stationary scenes for low frequency radar data via the Range Migration Algorithm (RMA). The RMA method inputs the original smeared signatures of scenes, so that the stationary scattering centers are defocused along curved arcs. These methods focus these curved arcs to be points for the special case of idealized point scattering. Other focusing methods correct only the cross-range defocus components. Thus, they do not correct residual range migration effects, resulting in reduced image quality due to residual defocus at lower radar frequencies. Other researchers[6] have investigated methods for focusing targets for which range migration effects have caused down-range smearing in the SAR signatures.

Recent studies[7] have analyzed the signatures of specific moving target examples in SAR image data. An investigation of the morphology of mover smears for general maneuvering targets has been presented previously.[1] This study investigates range migration effects for spotlight-mode SAR, which is an imaging mode[8,9] that yields a high image resolution at the expense of lower coverage rate. This analysis applies a power series expansion to local subaperture SAR images in order to generate general analytic equations for the shape of surface mover smears. Specifically, this study analyzes spotlight SAR for broadside imaging and a straight and level radar flight path. This investigation has yielded analytic non-parametric expressions for smear signature shapes for surface targets with arbitrary motion profiles.

The fundamental analytics in the previous analysis[1,10] is based upon analytic equations for the central contour shape for the signature induced by a moving target within SAR sub-aperture images. Subaperture SAR images has been utilized by various researchers[11–13] for multiple purposes.

Previous analyses[1,10,14] demonstrate the accuracy of the predictive equations for the central smear contour shape for a number of special cases. One of these examples is the case of a surface target that is moving with a constant speed while undergoing a turning maneuver. In addition, the current analysis examines the effects on the predicted and actual SAR mover signatures of varying the target turning radius. To do so, free parameters in the analytic predictive equations are varied and the resulting plots are analyzed.

## 2. IMAGE FORMATION

The radar platform transmits and receives a waveform for each location along the synthetic aperture and forms the complex $I$ and $Q$ channels. The complex phase history data are formed from these data, including the complex magnitude of the two channels and the phase via the arctan of the ratio of $Q$ over $I$. These phase history data are measured at the various frequencies $f_{m'}$ spanned by the radar waveforms and at the different values of slow-time $t$ along the synthetic aperture. These operations give the down-converted, frequency-domain measurement data in the original format:

$$\tilde{G}(f_{m'}, t_{n'}) = \Sigma_i \sigma_i \exp(-j2\pi\Delta R_i(t_{n'})2f_{m'}/c). \tag{1}$$

Here, the path difference relative to the ground reference point (GRP) at the center of the scene is defined by

$$\Delta R_i(t_{n'}) \equiv R_i(\theta(t_{n'}), \varphi(t_{n'})) - R_0(\theta(t_{n'}), \varphi(t_{n'})). \tag{2}$$

The polar-formatted frequency-domain data are related to the original phase history data by a one-dimensional (1-D) Fourier transform along the range dimension.

The complex-valued $\tilde{G}$ in (1) determine the real (i.e., in phase) and imaginary (i.e., quadrature) components of the sub-band centered on frequency sample value $f_{m'}$ for a particular slow-time sample value $t_{n'}$. The constant $c$ is the light speed, and $j = \sqrt{-1}$ is the imaginary constant. The factor of 2 provides for the two-way radar propagation.

The summation over $i$ in (1) allows for the effects of a number of scattering centers for extended targets. The quantity $R_i(\theta(t_{n'}), \varphi(t_{n'}))$ is the distance from the radar at slow-time $t_{n'}$ to the $i$th scattering center characterized by the complex-valued reflectivity $\sigma_i$:

$$\begin{aligned} &R_i(\theta(t_{n'}), \varphi(t_{n'})) \\ &= \sqrt{\{X(t_{n'}) - \alpha(t_{n'})\}^2 + \{Y(t_{n'}) - \beta(t_{n'})\}^2 + \{Z(t_{n'})\}^2} \end{aligned} \tag{3}$$

Likewise, $R_0(\theta(t_{n'}), \varphi(t_{n'}))$ is the distance from the radar to the GRP at the $\{x, y, z\} = \{0, 0, 0\}$ coordinate origin, i.e.,

$$R_0(\theta(t_{n'}), \varphi(t_{n'})) = \sqrt{\{X(t_{n'})\}^2 + \{Y(t_{n'})\}^2 + \{Z(t_{n'})\}^2}. \tag{4}$$

The following functions delineate the ground range and the ground cross-range components of the spatial frequency, i.e.,

$$\xi_m(f_{m'}, t_{n'}) \equiv \frac{2f_{m'}}{c} \cos(\theta(t_{n'})) \cos(\varphi(t_{n'})), \tag{5}$$

$$\eta_m(f_{m'}, t_{n'}) \equiv \frac{2f_{m'}}{c} \cos(\theta(t_{n'})) \sin(\varphi(t_{n'})). \tag{6}$$

A polar-to-rectangle resampling procedure[8] is applied to obtain the Cartesian-sampled data, i.e.,

$$\tilde{G}(f_{m'}, t_{n'}) \underset{\text{pol}}{\rightarrow} G(\xi_m, \eta_n). \tag{7}$$

Here, $G(\xi_m, \eta_n)$ is the complex-valued frequency-domain Cartesian data. Here, there are $M$ discrete resampled values of $\xi_m$, and there are $N$ discrete resampled values of $\eta_n$. Then, a 2D discrete Fourier transform (DFT) yields the spotlight-mode SAR image:

$$G(\xi_m, \eta_n) \underset{\text{2D DFT}}{\longleftrightarrow} b(x_k, y_\ell). \tag{8}$$

## 3. SIGNATURE PREDICTIONS

For the following results, the radar is assumed to travel on a straight and level flight path with constant speed and a broadside radar imaging geometry, yielding the following in terms of a ground plane Cartesian coordinate system $\{x, y, z\}$:

$$X(t) = -X_0, \tag{9}$$

$$Y(t) = \pm V_0 t, \tag{10}$$

$$Z(t) = Z_0, \tag{11}$$

Here, $V_0$ is the speed of the radar platform, with $X_0$ is the radar ground range relative to the synthetic aperture center, and $Z_0$ is the radar elevation above the ground plane. The origin of the global Cartesian coordinates is selected to be the fixed aim-point on the ground to which the radar mainbeam is pointed during this spotlight SAR image collection, which is also referred to as the GRP. The positive sign in (10) denotes radar motion in the $+y$ direction, and the minus sign defines movement in the $-y$ direction. It is also useful to define the following constant:

$$\kappa_0 \equiv \mp \frac{X_0}{V_0}. \tag{12}$$

Recent analysis[1] applies a power series expansion to sub-aperture images to derive general expressions for the central contour of the smear signature for a surface target moving with an arbitrary motion profile. The present investigation considers the case of a surface target with a constant heading and a constant finite turning radius the SAR collection interval in more detail:

$$\alpha(t) = \bar{\alpha}_0 \mp \bar{\rho}_0 \sin(\bar{\phi}_0) \pm \bar{\rho}_0 \sin\left( \pm \frac{\bar{v}_0 t}{\bar{\rho}_0} + \bar{\phi}_0 \right), \tag{13}$$

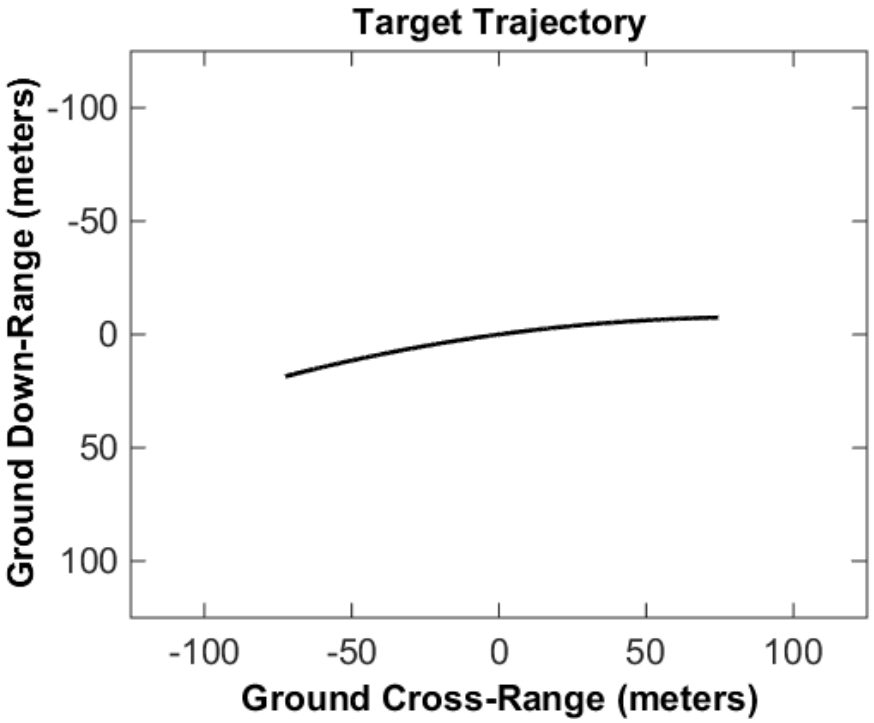


Figure 1. True target motion for a relatively large turning radius defined by the parameters $\{\bar{\alpha}_0 = 0.0\text{m}\}$, $\{\bar{\beta}_0 = 0.0\text{m}\}$, $\{\bar{v}_0 = 10.0\text{m/s}\}$, $\{\bar{\rho}_0 = 500.0\text{m}\}$, and $\{\bar{\phi}_0 = -80.0^\circ\}$

$$\alpha(t) = \bar{\alpha}_0 \pm \bar{\rho}_0 \cos(\bar{\phi}_0) \mp \bar{\rho}_0 \cos\left( \pm \frac{\bar{v}_0 t}{\bar{\rho}_0} + \bar{\phi}_0 \right), \tag{14}$$

with $\bar{\alpha}_0$, $\bar{\beta}_0$, $\bar{v}_0$, $\bar{\rho}_0$, and $\bar{\phi}_0$ all constant parameters.

Prior analytics[1] yields the following form for the predicted SAR signature of a turning, expressed in terms of the down-range and cross-range components:

$$x(\tau_s) = \bar{\alpha}_0 \mp \bar{\rho}_0 \sin(\bar{\phi}_0) \pm \left\{ \bar{\rho}_0 \mp \epsilon_s^2 \kappa_0 \bar{v}_0 \right\} \sin\left( \pm \frac{\bar{v}_0 \tau}{\bar{\rho}_0} + \bar{\phi}_0 \right) - \epsilon_s \kappa_0 \bar{v}_0 \cos\left( \pm \frac{\bar{v}_0 \tau}{\bar{\rho}_0} + \bar{\phi}_0 \right), \tag{15}$$

$$y(\tau_s) = \bar{\beta}_0 \pm \bar{\rho}_0 \cos(\bar{\phi}_0) \mp \left\{ \bar{\rho}_0 \mp \kappa_0 \bar{v}_0 \right\} \cos\left( \pm \frac{\bar{v}_0 \tau}{\bar{\rho}_0} + \bar{\phi}_0 \right) + \epsilon_s \kappa_0 \bar{v}_0 \sin\left( \pm \frac{\bar{v}_0 \tau}{\bar{\rho}_0} + \bar{\phi}_0 \right). \tag{16}$$

## 4. SIGNATURE RESULTS

This section examines the signatures that result for the case of a moving surface target undergoing a turning maneuver during the SAR collection time. For each of the following examples, the radar is assumed to be imaging with broadside geometry and a constant and level flight path. The selected radar trajectory parameters of (9) – (11) are a speed of $V_0 = 200\text{m/s}$, a ground range of $X_0 = 30\text{km}$, and an elevation of $Z_0 = 1\text{km}$. A total of 2000 waveforms with a center frequency of $f_c = 1.5\text{GHz}$ are transmitted and received at uniform intervals over a total collection time of $T_0 = 15\text{s}$. The radar bandwidth is 0.15GHz, and the signal processor collects complex I and Q data over 700 samples, which are uniformly sampled over the radar bandwidth.

For the first example, the parameters are selected to correspond to motion with a relatively large turning radius: $\{\bar{\alpha}_0 = 0.0\text{m}\}$, $\{\bar{\beta}_0 = 0.0\text{m}\}$, $\{\bar{v}_0 = 10.0\text{m/s}\}$, $\{\bar{\rho}_0 = 500.0\text{m}\}$, and $\{\bar{\phi}_0 = -80.0^\circ\}$. A trajectory plot is shown in Figure 1. The radar beam is assumed to be pointed towards the left side of the platform. Figure 2 gives the resulting SAR smear signature for the case of a radar mainbeam that is pointed off of the port side.

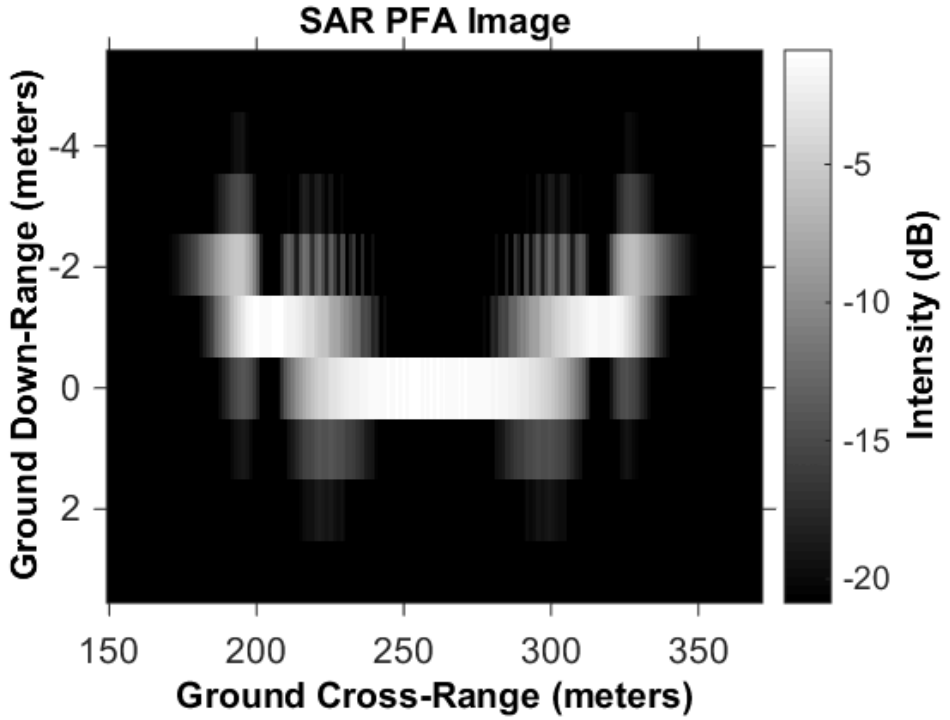


Figure 2. Resulting target signature for a relatively large turning radius defined by the parameters $\{\bar{\alpha}_0 = 0.0\text{m}\}$, $\{\bar{\beta}_0 = 0.0\text{m}\}$, $\{\bar{v}_0 = 10.0\text{m/s}\}$, $\{\bar{\rho}_0 = 500.0\text{m}\}$, and $\{\bar{\phi}_0 = -80.0^\circ\}$ for the case of a leftward pointing radar mainbeam

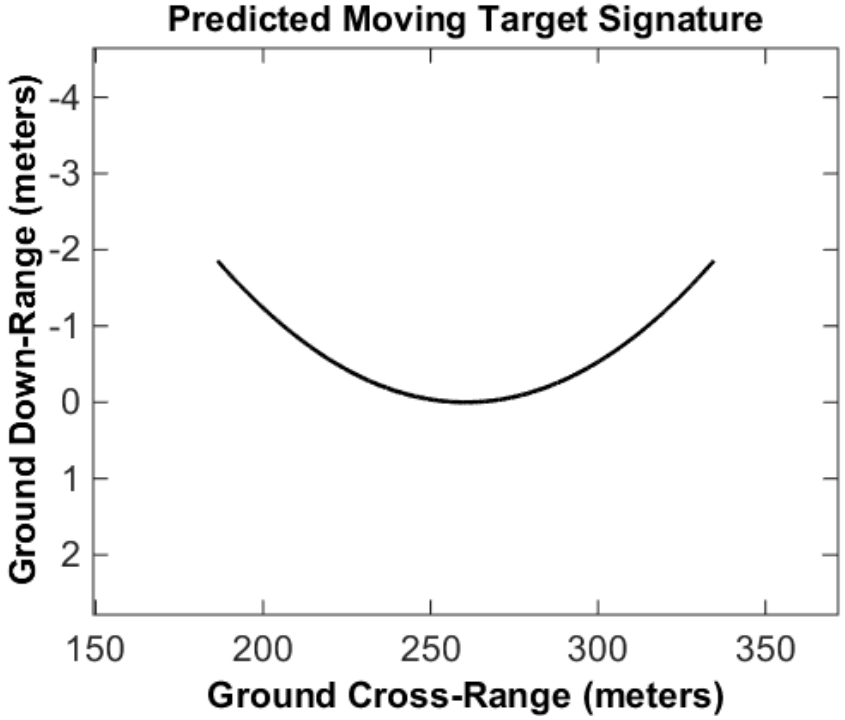


Figure 3. Corresponding predicted target signature for a relatively large turning radius defined by the parameters $\{\bar{\alpha}_0 = 0.0\text{m}\}$, $\{\bar{\beta}_0 = 0.0\text{m}\}$, $\{\bar{v}_0 = 10.0\text{m/s}\}$, $\{\bar{\rho}_0 = 500.0\text{m}\}$, and $\{\bar{\phi}_0 = -80.0^\circ\}$ for the case of a leftward pointing radar mainbeam

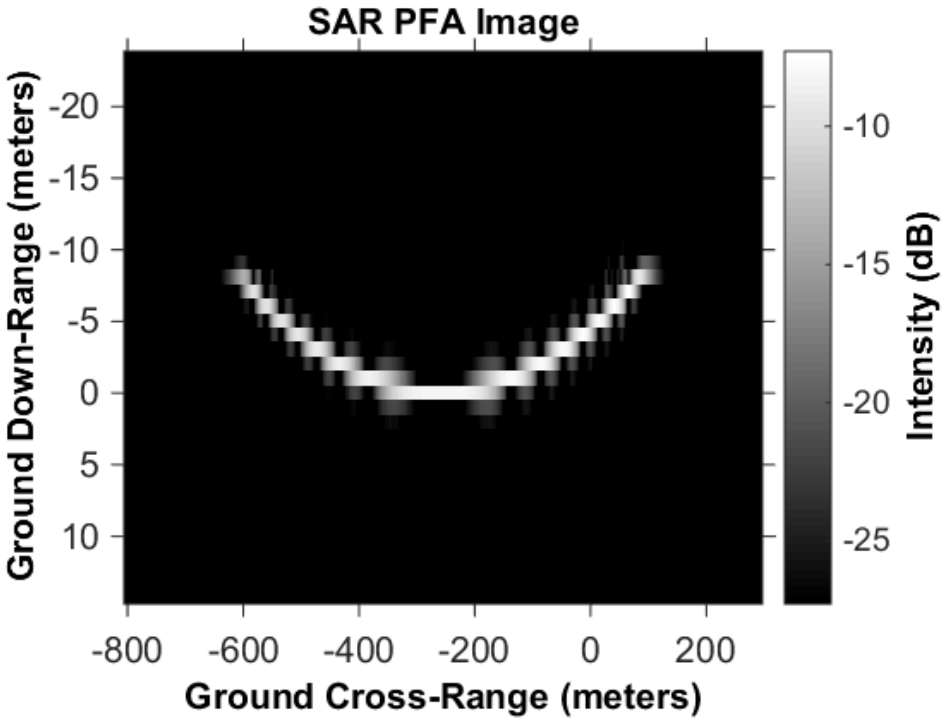


Figure 4. Resulting target signature for a relatively large turning radius defined by the parameters $\{\bar{\alpha}_0 = 0.0\text{m}\}$, $\{\bar{\beta}_0 = 0.0\text{m}\}$, $\{\bar{v}_0 = 10.0\text{m/s}\}$, $\{\bar{\rho}_0 = 500.0\text{m}\}$, and $\{\bar{\phi}_0 = -80.0^\circ\}$ for the case of a rightward pointing radar mainbeam

This analysis gives an accurate match between the predicted signatures of Figure 3 and the actual target signature of Figure 2. Therefore, this analysis yields further verification of the predictive signature theory derived in the original work.[1]

Figures 2 and 3 have presented the SAR smears for the case of a radar that is pointed off of the port (i.e., left) side of the radar platform. In contrast, Figures 4 and 5 compare the actual and predicted SAR smear signatures for the case of the same target as in the previous example, but with the radar mainbeam is pointed off of the starboard (i.e., right) side of the radar platform. Again, there is excellent agreement between the predicted and actual SAR signatures in terms of smear position, extent, and shape.

The next set of plots considers a target that is executing a turning maneuver, but with a tighter turning radius that is one-half that of the previous example set. Thus, these latter examples consider the parameter set: $\{\bar{\alpha}_0 = 0.0\text{m}\}$, $\{\bar{\beta}_0 = 0.0\text{m}\}$, $\{\bar{v}_0 = 10.0\text{m/s}\}$, $\{\bar{\rho}_0 = 250.0\text{m}\}$, and $\{\bar{\phi}_0 = -80.0^\circ\}$. Only the parameter $\{\bar{\rho}_0 = 250.0\text{m}\}$ has a different value. The corresponding true target trajectory is shown in Figure 6.

Figures 7 and 8 present the SAR smears for the case of a radar that is pointed off of the port side. This smear signature has a significantly greater extent is comparison to that of the first example in Figures 2 and 3.

Figures 9 and 10 compare the actual and predicted SAR smear signatures for the case of a tighter turning radius, i.e., $\{\bar{\alpha}_0 = 0.0\text{m}\}$, $\{\bar{\beta}_0 = 0.0\text{m}\}$, $\{\bar{v}_0 = 10.0\text{m/s}\}$, $\{\bar{\rho}_0 = 250.0\text{m}\}$, and $\{\bar{\phi}_0 = -80.0^\circ\}$, but with the radar pointed starboard. As with the previous examples, there is excellent agreement between the predicted and actual SAR signatures in terms of smear position, extent, and shape. This example yields a significantly increase smear extent in comparison to that of the second example of Figures 4 and 5.

## 5. CONCLUSIONS

This paper has examined the signatures of surface moving targets that are executing turning maneuvers during the SAR collection interval. The signatures smears obtained using image formation applied to simulated radar data were consistent with the analytic predictive equations based upon theory. The effects of the size of the

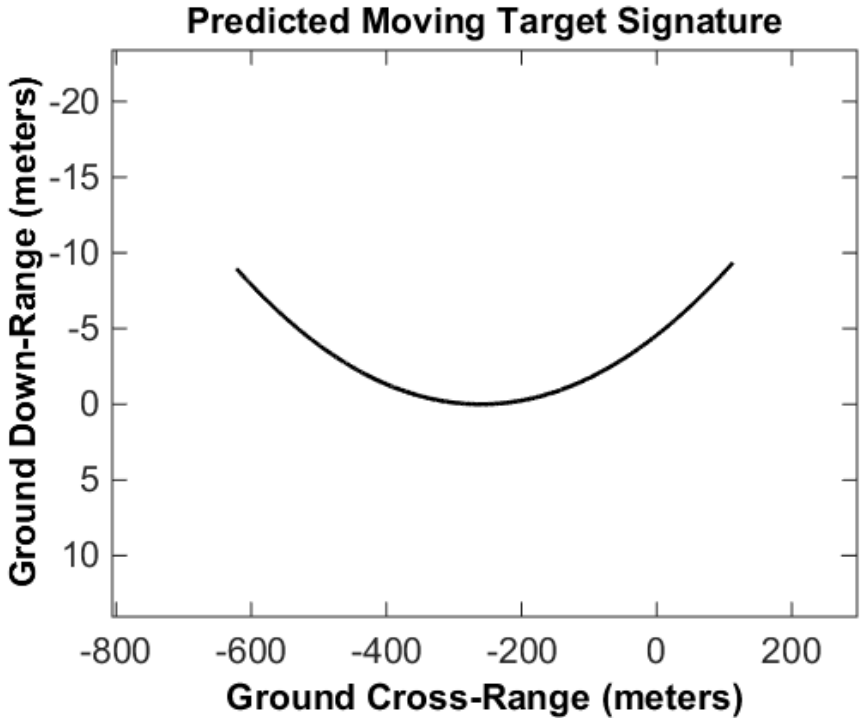


Figure 5. Corresponding predicted target signature for a relatively large turning radius defined by the parameters $\{\bar{\alpha}_0 = 0.0\text{m}\}$, $\{\bar{\beta}_0 = 0.0\text{m}\}$, $\{\bar{v}_0 = 10.0\text{m/s}\}$, $\{\bar{\rho}_0 = 500.0\text{m}\}$, and $\{\bar{\phi}_0 = -80.0^\circ\}$ for the case of a rightward pointing radar mainbeam

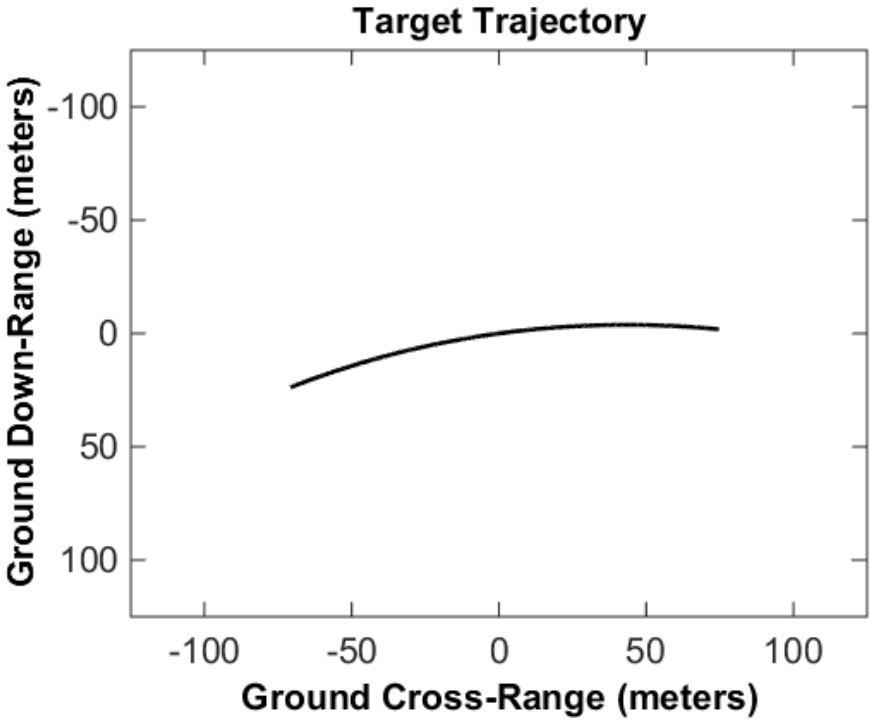


Figure 6. True target motion for a smaller turning radius defined by the parameters $\{\bar{\alpha}_0 = 0.0\text{m}\}$, $\{\bar{\beta}_0 = 0.0\text{m}\}$, $\{\bar{v}_0 = 10.0\text{m/s}\}$, $\{\bar{\rho}_0 = 250.0\text{m}\}$, and $\{\bar{\phi}_0 = -80.0^\circ\}$

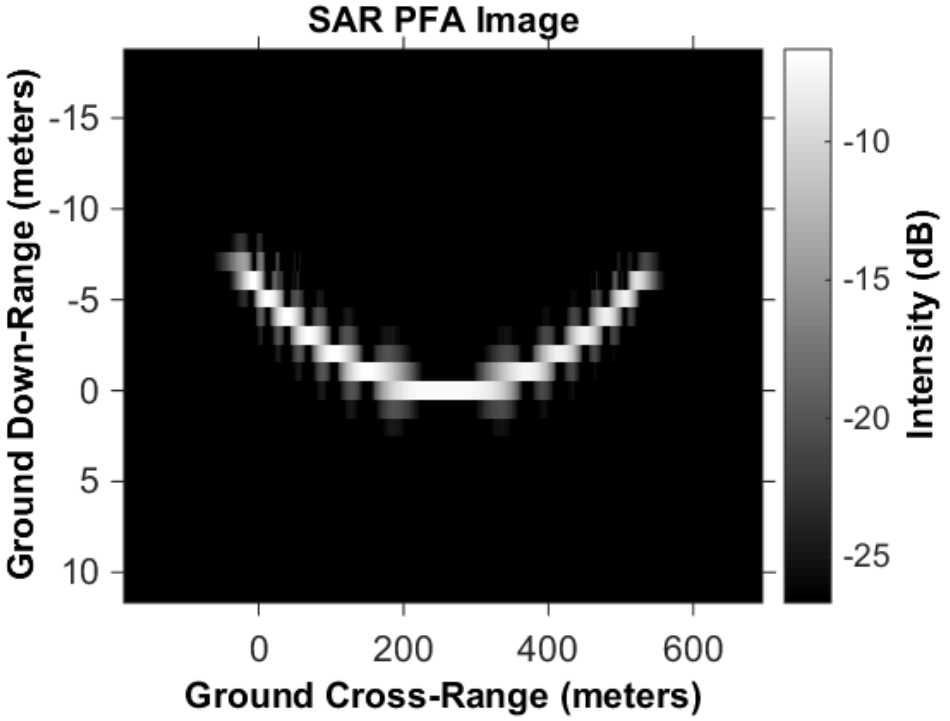


Figure 7. Resulting target signature for a smaller turning radius defined by the parameters $\{\bar{\alpha}_0 = 0.0\text{m}\}$, $\{\bar{\beta}_0 = 0.0\text{m}\}$, $\{\bar{v}_0 = 10.0\text{m/s}\}$, $\{\bar{\rho}_0 = 250.0\text{m}\}$, and $\{\bar{\phi}_0 = -80.0^\circ\}$ for the case of a leftward pointing radar mainbeam

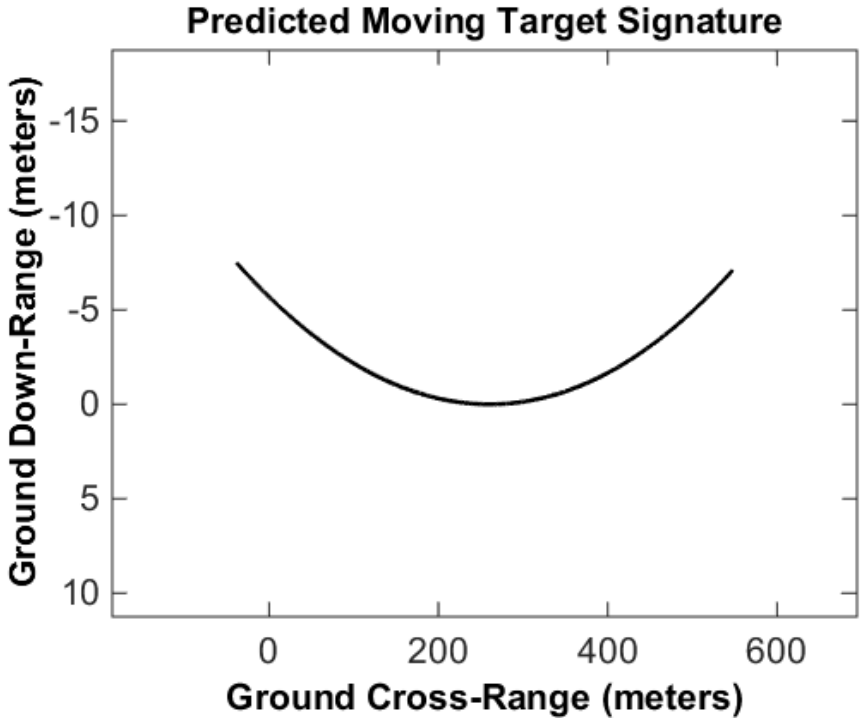


Figure 8. Corresponding predicted target signature for a smaller turning radius defined by the parameters $\{\bar{\alpha}_0 = 0.0\text{m}\}$, $\{\bar{\beta}_0 = 0.0\text{m}\}$, $\{\bar{v}_0 = 10.0\text{m/s}\}$, $\{\bar{\rho}_0 = 500.0\text{m}\}$, and $\{\bar{\phi}_0 = -80.0^\circ\}$ for the case of a leftward pointing radar mainbeam

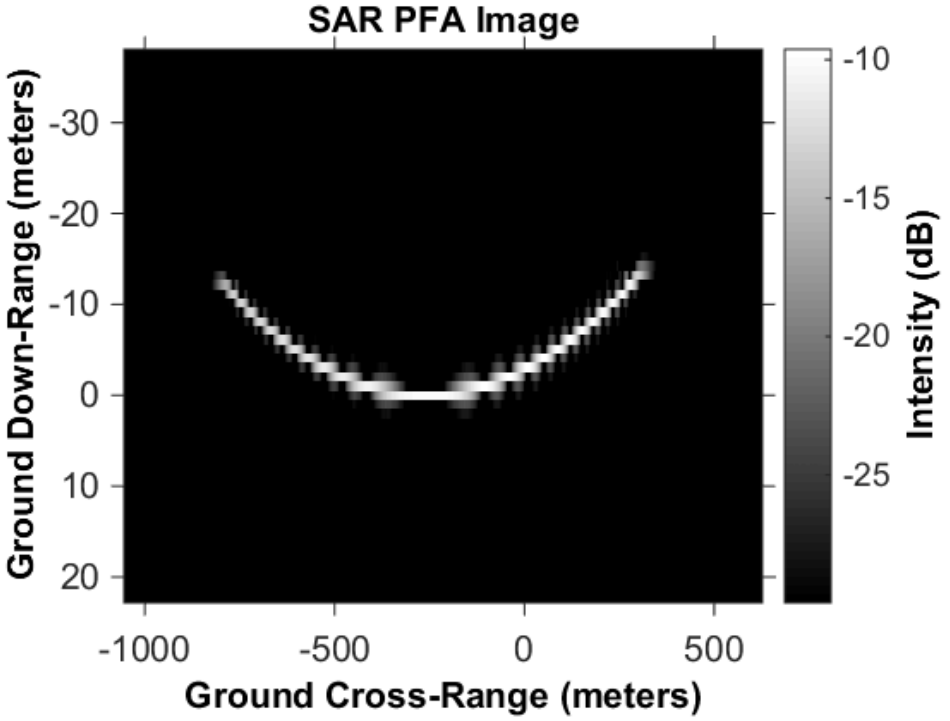


Figure 9. Resulting target signature for a smaller turning radius defined by the parameters $\{\bar{\alpha}_0 = 0.0\text{m}\}$, $\{\bar{\beta}_0 = 0.0\text{m}\}$, $\{\bar{v}_0 = 10.0\text{m/s}\}$, $\{\bar{\rho}_0 = 500.0\text{m}\}$, and $\{\bar{\phi}_0 = -80.0^\circ\}$ for the case of a rightward pointing radar mainbeam

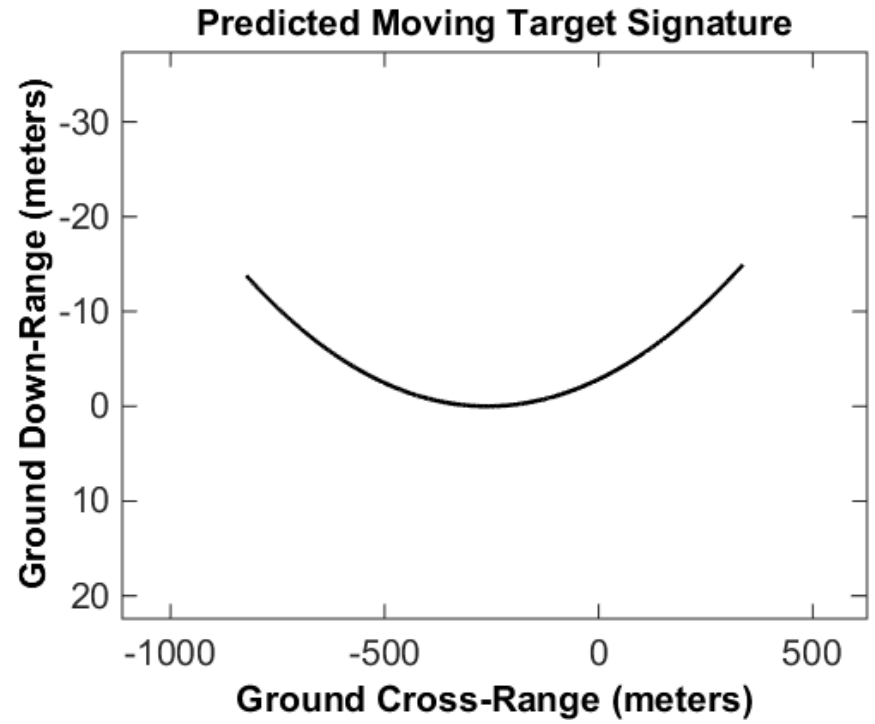


Figure 10. Corresponding predicted target signature for a smaller turning radius defined by the parameters $\{\bar{\alpha}_0 = 0.0\text{m}\}$, $\{\bar{\beta}_0 = 0.0\text{m}\}$, $\{\bar{v}_0 = 10.0\text{m/s}\}$, $\{\bar{\rho}_0 = 500.0\text{m}\}$, and $\{\bar{\phi}_0 = -80.0^\circ\}$ for the case of a rightward pointing radar mainbeam

turning radius and the direction of the radar pointing were examined in this analysis. Turning maneuvers were found to create very long smears in many cases, which follows from the strong effects of target acceleration on signature extent in comparison to that due to target velocity.[1]

## Acknowledgment

DoD Distribution Statement A: Unlimited Distribution. The views expressed in this document are those of the authors and do not reflect the official policy or position of the Department of Defense or the U.S. Government.

## REFERENCES

[1] D. A. Garren, "Smear signature morphology of surface targets with arbitrary motion in spotlight synthetic aperture radar imagery," *IET Radar, Sonar and Navigation*, vol. 8, no. 5, pp. 435–448, Jun 2014.

[2] R. P. Perry, R. C. DiPietro, and R. L. Fante, "SAR imaging of moving targets," *IEEE Transactions on Aerospace and Electronic Systems*, vol. 35, no. 1, pp. pp. 188–200, Jan 1999.

[3] R. K. Raney, "Synthetic aperture imaging radar and moving targets," *IEEE Transactions on Aerospace and Electronic Systems*, vol. 7, no. 3, pp. pp. 499–505, May 1971.

[4] J. K. Jao, "Theory of synthetic aperture radar imaging of a moving target," *IEEE Transactions on Geoscience and Remote Sensing*, vol. 39, no. 9, pp. 1984 –1992, Sep 2001.

[5] R. H. Stolt, "Migration by fourier transform," *Geophysics*, vol. 43, pp. 23–48, 1978.

[6] S. Rahman, "Focusing moving targets using range migration algorithm in ultra wideband low frequency synthetic aperture radar," Master's thesis, Blekinge Institue of Technology, Jun 2010.

[7] D. Garren, J. W. Scrofani, M. Tummala, and J. C. McEachen, "Target migration path morphology of moving targets in spotlight sar," *Proc. of SPIE Vol. 8746 87460B-7: "Algorithms for Synthetic Aperture Radar Imagery XX" of the SPIE Defense, Security, and Sensing Conference held 29 April - 3 May 2013 in Baltimore, Maryland; USA*, May 2013.

[8] C. V. Jakowatz Jr., D. E. Wahl, P. H. Eichel, D. C. Ghiglia, and P. A.Thompson, *Spotlight-Mode Synthetic Aperture Radar: A Signal Processing Approach.* Norwell, MA, USA: Kluwer Academic Publishers, 1996.

[9] W. G. Carrara, R. S. Goodman, and R. M. Majewski, *Spotlight Synthetic Aperture Radar Signal Processing Algorithms.* Norwood, MA, USA: Artech House, 1995.

[10] D. A. Garren, "Theory of two-dimensional signature morphology for arbitrarily moving surface targets in squinted spotlight synthetic aperture radar," *To appear in the IEEE Transactions on Geoscience and Remote Sensing.*

[11] J. Zhang, J. Xu, Y. Peng, and X. Wang, "Speckle filtering of SAR images based on sub-aperture technique and principal component analysis," *Communications and Information Technology 2005. ISCIT 2005. IEEE International Symposium on*, vol. 2, pp. 1217–1222, Oct 2005.

[12] M. Soumekh, "A system model and inversion for synthetic aperture radar imaging," *IEEE Transactions on Image Processing*, vol. 1, no. 1, pp. 64–76, Jan 1992.

[13] ——, "Digital spotlighting and coherent subaperture image formation for stripmap synthetic aperture radar," *Image Processing, 1994, Proceedings, ICIP-94, IEEE International Conference*, vol. 1, pp. 476–480, Nov 1994.

[14] D. A. Garren, "Signatures of braking surface targets in spotlight synthetic aperture radar," *Proceedings of 2014 Sensor Signal Processing for Defence, held in Edinburgh, UK, on 08-09 September 2014*, pp. 51–55, Sep 2014.